Laminar fluid and heat flow through an opened rectangular cooling chamber

T. S. Lee
Department of Mechanical and Production Engineering, National University of Singapore, Singapore

A numerical model was developed to study the laminar flow and temperature fields in a flow-through rectangular cooling chamber. Hot fluid is introduced into one end of the chamber and withdrawn from the other end. The top of the chamber is exposed to the atmosphere for cooling and the remaining side-walls are all insulated. The Reynolds number R_o considered is in the range of 100 to 1000 and the densimetric Froude number F_o considered is in the range of 0.5 to 50.0. Numerical experiments show that the flow fields and temperature profiles in the flow-through cooling chamber are strong functions of both the F_o and the R_o. Comparisons were also made with available experimental and prototype data.

Keywords: flow-through; cooling chamber; fluid motion; temperature fields

Introduction

Problems associated with the rejection of heat from a body of fluid have been the subject of much recent research due to their many important practical applications in the cooling of heated discharge from small heat-generating equipment and facilities or from large power plants.[1–27] The cooling of small confined environments in buildings or in equipment by forced or natural fluid convections[28–45] is also relevant to the present study. The method of heated fluid discharge and the resulting patterns of fluid flow within a body of fluid in an environment very often determine the mode of heat rejection and/or the quality of the returned cooling fluid. For large power plants, thermal discharges into cooling reservoirs are usually turbulent. However, for small heat-generating equipment and facilities, the inflows to cooling chambers may be laminar. Thus, it is often desirable to be able to understand the fluid motion in the cooling chamber due to the various modes of inflow, and to predict, as accurately as possible, whether the heat load from a heat source could be dissipated efficiently into and out of a given body of cooling fluid under certain conditions and limitations. For the present work, the study is limited to the laminar heated inflow into a cooling chamber from small heat-generating equipment or facilities. The cooling chambers are typically placed in an enclosed environment in a building, where the movement of air is usually minimal.

A similar numerical solution of the two-dimensional (2-D) mass, momentum, and energy equations for thermal discharge was obtained by Barry and Hoffman.[1] An explicit scheme was used to compute the temperature and velocity profiles in the receiving water body. Buoyancy, turbulence, and the equation of motion in the vertical plane were neglected. The solution is thus valid for very shallow bodies of water. In another study, Boericke and Hall[2] analyzed the behavior of the hydraulic and thermal dispersion of heated water discharged into an irregular estuary. The model is also based on the shallow-water approximation to the momentum equations in two dimensions. The vertical variations in velocity and temperature are neglected. For study of the vertical variations of velocity and temperature, Stefan[3] modeled the spread of heated water over a 2-D vertical trapezoidal section of a lake. The fluid dynamics and temperature fields in the lake were numerically simulated by means of a finite-difference procedure. Inflow is allowed at the surface on one end of the reservoir, and outflow occurs at the opposite end. The reservoir inflow is set at a given temperature and velocity so as to simulate the thermal discharge from a power-generating facility. There are also numerous other numerical and experimental studies of large thermal discharge problems,[4–27] but very few considered the variations of temperature and velocity fields in the vertical plane of the cooling chambers for the dissipation of heat from the smaller heat-generating facilities. These vertical variations of temperature and velocity profiles are important in the present study of cooling chambers in an enclosed building environment. The typical aspect ratio of the cooling chamber in an enclosed environment is of the order of $L/D \leq 10$.

Laminar fluid convection studies similar to the present work can be extended to include the natural and forced convection studies in enclosures,[28–45] such as the forced convective cooling of the printed circuit board in a confined space by Davalath and Bayazitoglu;[32] the numerical studies of inflow into air-conditioned rooms in a vertical plane by Nielsen;[38] and the studies of convective heat and fluid flow in enclosures of various shapes.[34–37] In the study of inflow into an air-conditioned room, for example, instead of hot fluid being discharged into an enclosed environment, cooled air is introduced into a room.

Model and governing equations

The model of the cooling chamber studied here consists of a 2-D rectangular region, as shown in Figure 1. The inlet of warm fluid is at the surface of the chamber and the outlet of the cooler liquid is specified at some depth D_e below the free surface. The dimensions d_o and d_e specify the widths of the inlet and outlet of the cooling chamber. Heat is convected into the chamber at the inlet and is lost through the surface and by convection at thd outlet. All the other walls are assumed adiabatic. In the analysis of the flow-through cooling chamber, the following assumptions were made: (1) flow in the chamber has reached a steady state; (2) temperature variations in the chamber are sufficiently small that the Boussinesq approximation is valid;

Address reprint requests to Dr. Lee at the Department of Mechanical and Production Engineering, National University of Singapore, Singapore, 0511.

Received 9 October 1990; accepted 28 January 1991

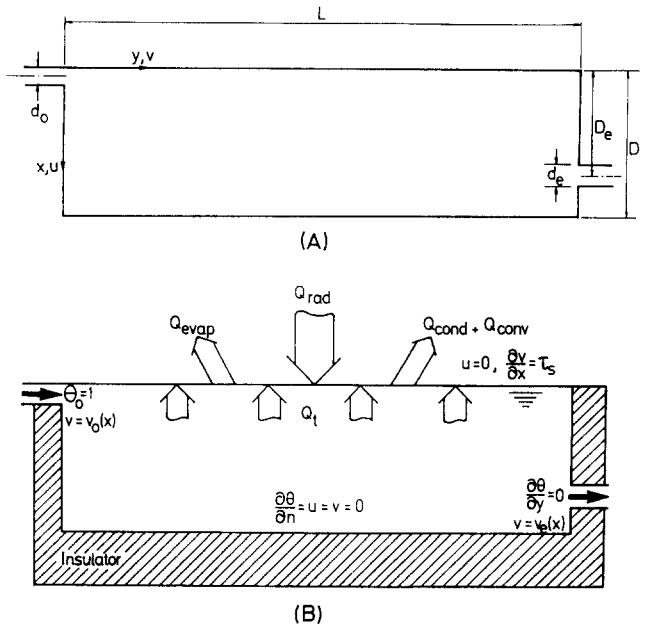

Figure 1 The model rectangular cooling chamber. (A) Coordinate system; (B) boundary conditions

(3) internal energy generation is absent; (4) the heat capacity of the fluid is sufficiently large that the temperature of the fluid is negligibly affected by friction; and (5) free surface elevation remains constant and the rigid-lid assumption is being made.[20,21,23]

The governing equations describing the laminar flow motion in the above cooling chamber are those expressing conservation of mass, momentum, and energy given by

$$\nabla \cdot \tilde{\mathbf{u}} = 0 \tag{1}$$

$$\frac{D\tilde{\mathbf{u}}}{Dt} = -\frac{\nabla p}{\rho_o} + \nu \nabla^2 \tilde{\mathbf{u}} + \frac{\rho}{\rho_o}\tilde{g} \tag{2}$$

$$\frac{DT}{Dt} = \alpha \nabla^2 T \tag{3}$$

and the Boussinesq approximation

$$\rho = \rho_o[1 - \beta(T - T_o)] \tag{4}$$

in which $\tilde{\mathbf{u}}$ is the velocity vector. The symbols ρ, g, ν, and α denote, respectively, the density, gravitational acceleration, kinematic viscosity, and thermal diffusivity; p and T are the pressure and the temperature of the fluid. Subscript 'o' indicates some reference state, say that of the inlet warm water. The coefficient β in the density–temperature relationship is taken as constant.

Taking curl of Equation 2 to eliminate the pressure term and to express the equation in terms of vorticity ($\tilde{\zeta}$) gives

$$\frac{\partial \tilde{\zeta}}{\partial t} + \nabla \times (\tilde{\zeta} \times \tilde{\mathbf{u}}) = \nu \nabla^2 \tilde{\zeta} - \nabla \times \left(\frac{\rho}{\rho_o} \hat{g} \right) \tag{5}$$

where the vorticity is defined as

$$\tilde{\zeta} = \nabla \times \tilde{\mathbf{u}} \tag{6}$$

In terms of the stream function ($\tilde{\psi}$),

$$\tilde{\mathbf{u}} = \nabla \times \tilde{\psi} \tag{7}$$

then

$$\zeta = -\nabla^2 \tilde{\psi} \tag{8}$$

Let the dimensionless parameters be defined as $x^* = x/X$, $y^* = y/Y$, $\theta = (T - T_{ref})/(T_o - T_{ref})$, $\tilde{\mathbf{u}}^* = \tilde{\mathbf{u}}/V_o$, $\tilde{\psi}^* = \tilde{\psi}/(V_o d_o)$, $\tilde{\zeta}^* = \tilde{\zeta}/(V_o d_o)$. X, Y are scaling factors for the x- and y-coordinates, respectively, and T_{ref} is a reference temperature. Define also inlet Reynolds number $R_o = V_o d_o/\nu$; densimetric Froude number $F_o = V_o/[g d_o(\rho_{ref} - \rho_o)/\rho_o]^{1/2}$; Prandtl number $\mathrm{Pr} = \nu/\alpha$; and aspect ratios $A_1 = (d_o/X)$ and $A_2 = (d_o/Y)$. The governing equations become

$$\tilde{\zeta}^* = -\nabla^{*2} \tilde{\psi}^* \tag{9}$$

$$\tilde{\mathbf{u}}^* = \nabla^* \times \tilde{\psi}^* \tag{10}$$

$$\frac{\partial \tilde{\zeta}^*}{\partial t^*} + \nabla^* \times (\tilde{\zeta}^* \times \tilde{\mathbf{u}}^*) = \frac{1}{R_o} \nabla^{*2} \tilde{\zeta}^* - \frac{1}{F_o^2} (\nabla^* \times \theta \hat{g}^*) \tag{11}$$

$$\frac{\partial \theta}{\partial t^*} + \nabla^* \cdot (\tilde{\mathbf{u}} \theta) = \frac{1}{R_o \mathrm{Pr}} \nabla^{*2} \theta \tag{12}$$

For the 2-D problem,

$$\nabla^* = A_1 \frac{\partial}{\partial x^*} \hat{i} + A_2 \frac{\partial}{\partial y^*} \hat{j}$$

(From here on, the * representing dimensionless variables and quantities are omitted for simplicity.)

Notation

A	Aspect ratio, $A = L/D$
d_e	Width of the exit opening of the chamber
d_o	Width of inlet opening of the chamber
D	Depth of chamber
D_e	Depth of submergence of exit opening
F_o	Densimetric Froude number, $F_o = V_o/\{g d_o(\rho - \rho_o)/\rho_o\}^{0.5}$
g	Gravitational constant
L	Length of chamber
L_c	Characteristic length, $L_c = (L \times D)^{1/2}$
M, N	Mesh sizes
Pr	Prandtl number, $\mathrm{Pr} = \nu/\alpha$
P	Pressure
R_o	Reynolds number $R_o = V_o d_o/\nu$
Δt	Time increment
T	Temperature
T_a	Temperature of ambient air
T_E	Equilibrium liquid temperature
T_o	Temperature of inlet hot fluid
u	Velocity in the x-direction
v	Velocity in the y-direction
x, y	Two-dimensional rectangular coordinates
∇^2	Laplace operator

Greek symbols

α	Thermal diffusivity
β	Coefficient of volumetric expansion
θ	Dimensionless temperature
ν	Kinematic viscosity
ρ_o	Reference density
ψ	Stream function
ζ	Vorticity

Boundary conditions

Thermal boundary conditions

Rigid boundaries are assumed adiabatic; therefore, $\partial\theta/\partial n=0$, where n is the direction normal to the boundary. The temperature at the inlet is assumed to be uniform. At the outlet, heat is assumed to be transferred across this boundary by convection alone (i.e., $\partial\theta/\partial y=0$). The condition of $\partial\theta/\partial y=0$ also allows the temperature profile to develop with the flow field around the outlet region. At the ambient-liquid interface (Figure 1b), heat is transferred to the atmosphere by radiation (Q_{rad}), evaporation (Q_{evap}), and by conduction (Q_{cond}) and convection (Q_{conv}). The thermal condition at the chamber liquid surface, due to the heat load introduced from the inlet to the chamber, is therefore given by $\partial\theta/\partial x=K\theta_s$ at $x=0$. The value of K is primarily a function of the ambient air speed and the equilibrium (natural surface) temperature of the liquid body as defined by Edinger[5-7] and Jobson.[16]

Velocity boundary conditions

Velocities for the rigid nonslip walls are $u=v=0$. At the liquid reservoir surface, free surface elevation is assumed to remain constant, and the rigid-lid assumption is made.[20,21,23] Hence, $u=0$ at the free surface. The effect of air movement over the surface is modeled by a nondeformable surface shape, with ψ at the surface equal to a constant. The applied dimensionless wind stress due to air movement at the liquid surface, following Stefan,[24,25] is modeled as $\tau_s=-\partial v/\partial x$. In the absence of air movement, such as in an enclosed building environment, $\tau_s=0$. Velocities at the inlet and outlet region of the chamber reservoir are specified.

Stream function and vorticity boundary conditions

For a solid nonslip wall, $\psi=$constant and $\zeta=-A_n^2\,\partial^2\psi/\partial n^2$, where A_n is a nondimensionalized directional constant. At the free surface, $u=0$, ψ is a constant, and $\zeta=A_1\,\partial v/\partial x=$constant. Other boundary conditions for ψ and ζ must be derived from those for velocity in such a way that the solution obtained by using ψ and ζ is identical to that obtained by using u, v, and p.

Numerical solution procedures

Following Mallinson and de Vahl Davis[46] and Behnia, Wolfstein, and de Vahl Davis,[47] in order to speed up the convergence rate to steady-state solution of Equations 9–12, the approach adopted here is to introduce false transient factors (α_ϕ) into the time-derivative terms in Equations 11–12, which allow relative changes to be made in the time rates of change of ϕ ($\phi=\zeta$ or θ), i.e., to replace the time-derivative terms in Equations 11–12 with $1/\alpha_\phi\,\partial/\partial t$. Further change is also made to replace Equation 9 by the parabolic equation

$$\frac{1}{\alpha_\psi}\frac{\partial\psi}{\partial t}=\nabla^2\psi+\zeta \tag{13}$$

Numerical experiments show that, by using the above approach and with the proper choice of the α_ϕ values, a steady-state solution of Equations 9–13 can be reached with considerably less computational effort than with the set of steady-state elliptic equations.

The finite-difference solution of Equations 9–13 was obtained with a regular rectangular mesh system. The numerical procedure used is the ADI method originally proposed by Peaceman and Rachford.[48] All spatial derivatives are approximated by second-order-accurate central differences, and the convective terms of the governing equations are approximated by the second-order upwind differencing method. The resulting finite-difference equations were solved by a tridiagonal matrix inversion algorithm. For derivatives on the boundary, three-point forward or backward differences were used where appropriate. Estimates of boundary values of vorticity and temperature were obtained after each iteration in the ADI procedure and were used as more up-to-date approximations in the second half of the ADI procedure. The source term of each equation was calculated using the latest field value available.

It was initially hoped that the bulk of the results could be obtained using a 51×101 mesh, and that this mesh would be fine enough to show, with reasonable accuracy, the general features of the flow. At low Reynolds number and high densimetric Froude number, the solutions obtained were qualitatively acceptable. However, at high Reynolds number ($R_o>500$) and low densimetric Froude number ($F_o<1$), truncation errors were large, and unrealistic temperature fields resulted. A finer mesh of 101×201 was then used, and a marked improvement occurred in all the solutions. Further refinement in the mesh size produced little changes in the result. This degree of consistency was deemed acceptable here in view of the very large increase in computer cost required to obtain the minor benefits of any further increases in accuracy. Hence, unless otherwise specified, a 101×201 mesh was used in all the solutions described here.

For the numerical time-step (Δt) selection, it was found that a suitable Δt can be chosen empirically by examining the source term of the governing equation. If the source term of a governing equation is relatively small compared with the convection term and/or diffusion term (e.g., the ζ–ψ equation), or if the source term is zero (e.g., the θ-equation), then the Δt can be chosen according to the Courant–Friedrich–Lewy condition,[49] i.e., the upper limit on the Δt was determined by

$$\alpha_\phi\,\Delta t\le\frac{\Delta x}{|u_{max}|}\quad\text{and}\quad\alpha_\phi\,\Delta t\le\frac{\Delta y}{|v_{max}|} \tag{14}$$

whichever was the smaller. If the source term of the governing equation is very large, then the Δt for these equations is governed by a parameter λ, given by

$$\alpha_\phi\,\Delta t\le\lambda\Big/\left[2\left(\frac{1}{\Delta x^2}+\frac{1}{\Delta y^2}\right)\right] \tag{15}$$

where $1\le\lambda\le2$. The source term of the ζ transport equation lies between those described for Conditions (14) and (15). If the $F_o\gg1$, then the source term of the ζ-equation is relatively small. The motion is governed predominantly by the initial momentum of the jet. Condition (14) may then be used for the selection of the time step. However, if $F_o\le1$, then buoyancy may dominate the motion. The source term in the ζ-equation is relatively large, and Condition (15) is used for the time-step selection.

Results and discussions

In a study of this nature, it is inevitable that many results have been accumulated on computer output. It is obviously impossible to present all of these results here. In the discussion that follows, relatively few actual numerical results are presented; rather, emphasis is placed upon what is, in a sense, a broader view of the problem, namely, the analysis of the trends or expected behavior rather than particular results.

When fluid is drawn from a chamber, heated by some processes, and discharged back to the chamber to dissipate its heat load to the ambient, an orderly fluid motion can be observed within the cooling chamber. This fluid motion and

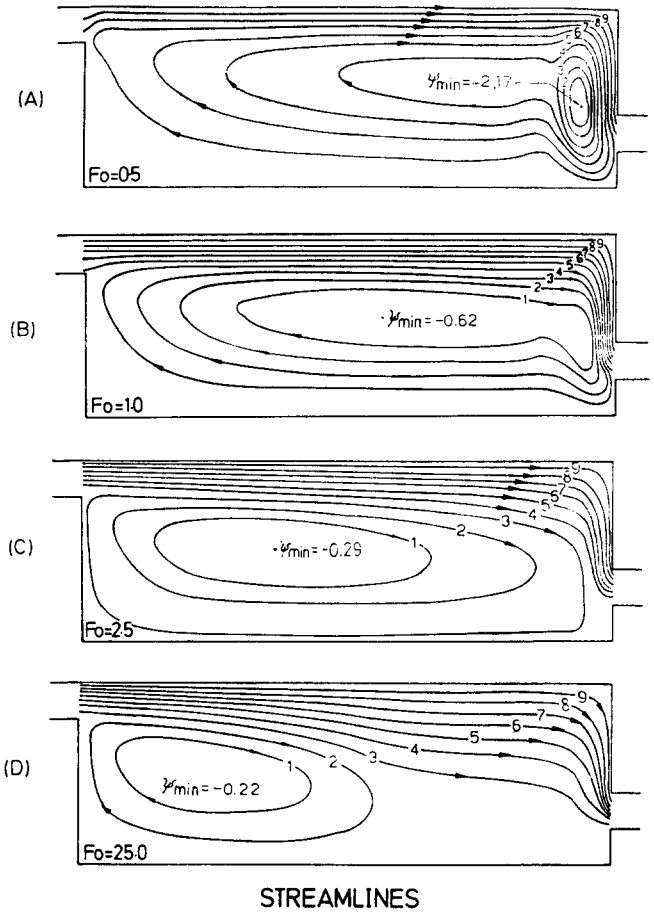

Figure 2 Effects of densimetric Froude number (F_o) on streamlines $R_o=500$, $L/D=10$. (A) $F_o=0.5$; (B) $F_o=1.0$; (C) $F_o=2.5$; (D) $F_o=25.0$

subsequent heat transfer from the surface of the cooling chamber is governed by the condition of discharge as well as by the shape and size of the chamber. Since fluid under normal conditions has a positive coefficient of thermal expansion, the warm fluid tends to rise to the surface and spread. This occurs because, regardless of the reduction of buoyancy by mixing, the warm inflow is always buoyant with respect to the ambient fluid. Thus, if the heated fluid is discharged near the surface of the cooling chamber, it will tend to remain afloat over the ambient fluid as a stratified layer. For the opened cooling chamber, the exposure of the upper surface of the incoming heated fluid to the atmosphere results in a larger temperature excess near the surface and thus allows greater temperature reduction by surface heat loss. If the heated surface fluid is discharged into the cooling chamber in such a way that minimum mixing occurs between the heated effluent and the receiving body of fluid, then heat dissipation to the atmosphere is at the highest rate, since the surface-layer temperature is at a maximum.

For surface discharges into a rectangular cooling chamber of $L/D=10$ and $D/d_o=5$ with varying F_o and R_o, the flow pattern and temperature profiles are shown in Figures 2 and 3 for $R_o=500$ held constant, and in Figures 4 and 5 for $F_o=1$ held constant. In the figures that follow, unless noted otherwise, the contour lines 1, 2, ..., 9 represent the contour level of 10%, 20%, ..., 90% of $(\phi_{max}-\phi_{min})$, where $\phi=\psi$ for the streamline contours and $\phi=\theta$ for the isotherm contours. It should be noted that all the results are plotted at a "reduced scaling"; hence, for chambers of $L/D=10$, the horizontal length is substantially compressed.

The two main dimensionless parameters used in studying the cooling chamber problem here (in which the inertia forces, buoyancy forces, and viscous forces control the phenomenon) are the densimetric Froude number F_o and the Reynolds number R_o. The following numerical experiments illustrate the role of F_o and R_o in establishing the flow pattern.

Variation of F_o has a significant effect on the trajectories of the buoyant inflow. Figures 2 and 3 show the effects of F_o on the streamline and isotherm contours for the cooling chamber numerical experiments. The incoming heated fluid spread from a buoyant plumelike discharge for $F_o=0.5$ and $F_o=1.0$ to a less buoyant jetlike discharge for $F_o=2.5$ and $F_o=25$.

For $F_o=0.5$ with $R_o=500$ (Figures 2a and 3a), the buoyant force of the incoming heated fluid is greater than its inertia force. With the inlet of the heated fluid positioned at the surface of the cooling chamber, the incoming heated fluid is observed to spread over the surface of the ambient fluid as a stratified layer as it enters the cooling chamber. As a result, the temperature excess at the surface near the inlet region is large. The 10% isotherm in the solution reaches the downstream boundary, indicating that the heated water has sufficient initial temperature excess and horizontal momentum to reach the outlet region without dissipating all its heat load to the ambient surrounding.

For $F_o=1.0$ with $R_o=500$ (Figures 2b and 3b), the buoyant

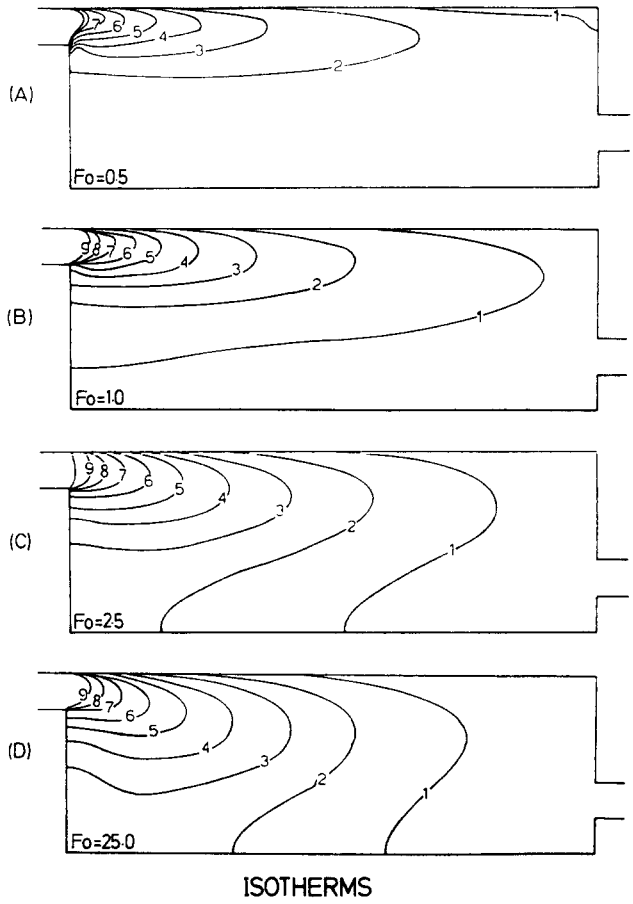

Figure 3 Effects of densimetric Froude number (F_o) on isotherms $R_o=500$, $L/D=10$. (A) $F_o=0.5$; (B) $F_o=1.0$; (C) $F_o=2.5$; (D) $F_o=25.0$

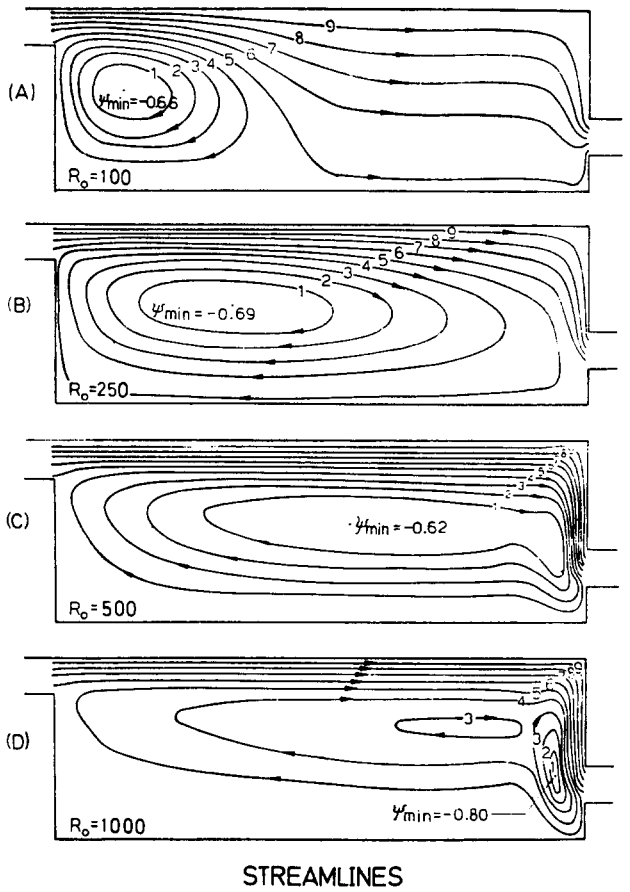

Figure 4 Effects of inlet Reynolds number (R_o) on streamlines $F_o=1.0$, $L/D=10$. (A) $R_o=100$; (B) $R_o=250$; (C) $R_o=500$; (D) $R_o=1000$

force of the incoming heated water is of the same order as its inertia force; the fluid is less heated compared with the same fluid at $F_o=0.5$. Equation 3b shows that the surface area of the cooling chamber considered is sufficient to dissipate all the heat load before the heated fluid reaches the outlet region. This is indicated by the area covered by the 10% isotherm contour for the surface inlet.

For $R_o=500$ with $F_o=2.5$ (Figures 2c and 3c) and $F_o=25$ (Figures 2d and 3d), the incoming heated fluid is relatively cool compared with the conditions when $F_o=0.5$ and $F_o=1.0$ for the same R_o. For $F_o=2.5$ and $F_o=25$, the inertia force of the incoming water is greater than its buoyant force. In this case, the incoming fluid does not have sufficient buoyancy (or temperature excess) to cause the fluid to spread as a stratified warm surface layer. Instead, the inflow tends to diffuse towards the middle of the chamber at some distance from the inlet. The tendency of this diffusion increases with increasing F_o. The magnitude of the initial mixing and dilution of the heated fluid near the inlet region also increases with increasing F_o. As a result, the initial excess temperature concentrations of the incoming heated fluid with $F_o=2.5$ and $F_o=25$ are not as large as those described for $F_o=0.5$ and $F_o=1.0$.

Further studies of the fluid motion and temperature profiles of the cooling chamber are shown in Figures 4 and 5 for varying R_o (with $F_o=1.0$). Much of the behavior displayed for an increase in R_o (with fixed F_o) is qualitatively similar to that for a decrease of F_o with R_o held constant. It should be cautioned here that as R_o varies at constant F_o, the values of $\Delta\rho_o=(\rho-\rho_o)$ in the definition of F_o can be different for different sets of numerical experiments without being evident in the solutions. For example, as the Reynolds number increased, V_o in $R_o=V_o d_o/\nu$ increases for fixed d_o and ν. For $F_o=V_o/[(\Delta\rho_o/\rho_o)gd_o]^{0.5}$ to remain constant with increasing V_o implies that $\Delta\rho_o$ has to increase proportionally. Thus, an increase in R_o with F_o held constant could also mean that $\Delta T_o=(T_o-T_E)$ has increased. Hence, following the above reasoning, much of the behavior displayed in Figures 4 and 5 for increasing R_o (with fixed F_o) is also qualitatively similar to the decreasing of F_o (with R_o fixed).

Comparison with findings of other investigators

Numerical models, while based on theoretical equations that represent the physical processes, are only approximations to the real physical processes involved. As a result, experimental evidence and field data are required to establish the accuracy and applicability of the numerical model. However, experiments suitable for direct comparison with the numerical results obtained here were few. One of these available for comparison was done by Pleasance.[44] The dimensionless parameters considered in the experiments were in the range of $F_o=0.70$ to 4.5 and $R_o=180$ to 1200. The results of the experiments and the corresponding numerical solutions are presented in Figures 6 and 7. The experimental results exhibit a strong forward current in a narrow layer near the surface with much smaller velocities beneath this layer, as indicated in Figure 6a. A reverse current occurs somewhere near the bottom of the reservoir to return

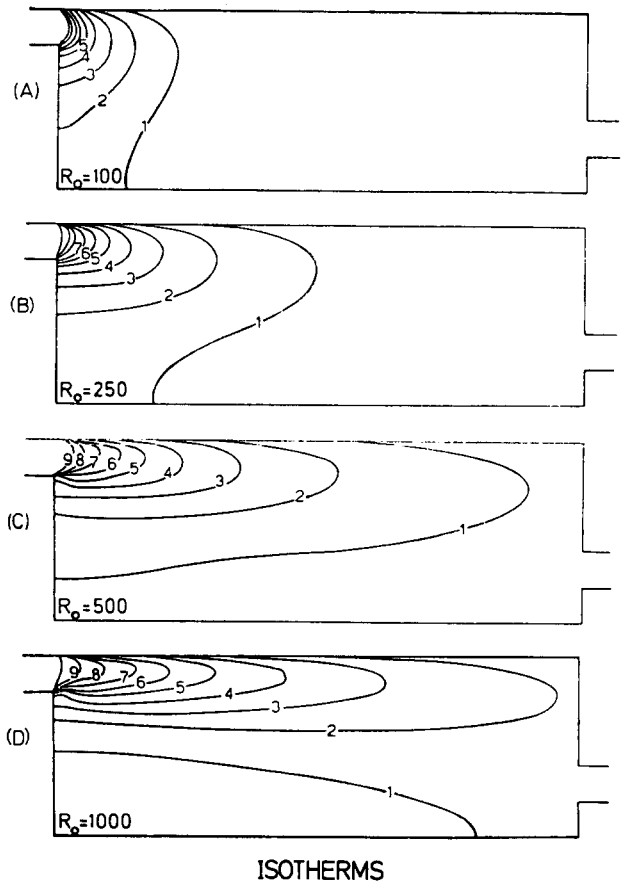

Figure 5 Effects of inlet Reynolds number (R_o) on isotherms $F_o=1.0$, $L/D=10$. (A) $R_o=100$; (B) $R_o=250$; (C) $R_o=500$; (D) $R_o=1000$

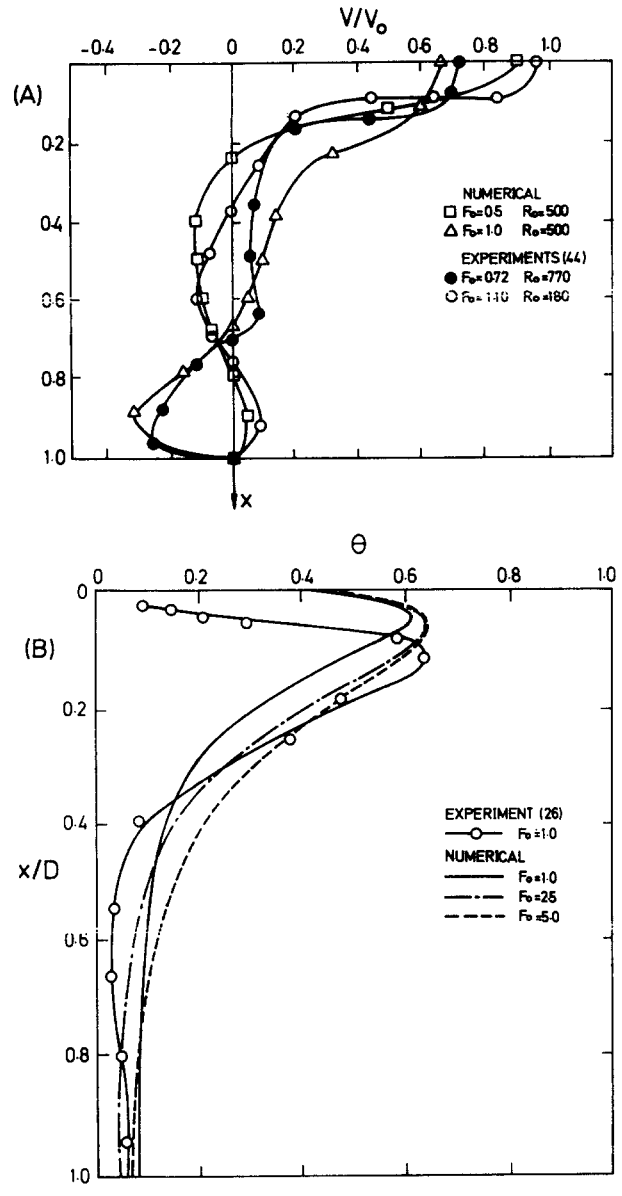

Figure 6 Comparison of experimental and field measurements with numerical experiments. (A) Vertical velocity profiles; (B) vertical temperature profiles

the mass flux entrained into the surface layer near the inlet region. This behavior is consistent with what was obtained in the numerical solutions, as indicated also in Figure 6a. There is some indication that, due to the influence of the physical side walls in the experiments and the 2-D constraint imposed on the numerical model, the strength of the reverse flow in the laboratory simulation of the problem was not as great as that predicted by the numerical model. Further study of the centerline temperature decay pattern away from the inlet region is shown in Figure 7. It shows that the profile of temperature decay away from the inlet region obtained from the numerical experiments closely followed those observed in the experiments. Studies of temperature distributions on prototype cooling reservoirs were also made by Coulter et al.,[4] Harbeck et al.,[9,10] Harleman and Stolzenbach,[11] Hayashi et al.,[12,13] Hindley, Miner, and Cayot,[14] Parker and Krenkel,[18] and others. The results presented vary considerably from site to site and are mainly for turbulent flow. Hence, no direct comparison of the turbulent thermal-discharge field data is made with the present laminar solution of a cooling-chamber flow problem. However, in general, the above data indicate large temperature gradients and significant vertical convection near the inlet to the cooling reservoir. One such vertical temperature profile obtained by Summers, Ellyett and Kennewell[26] at a site near an inlet to the cooling pond at a slow rate of discharge is shown in Figure 6b with some numerically obtained laminar vertical temperature profiles near the inlet to the cooling chamber. It can be seen that the dimensionless vertical temperature distribution near the inlet region of a prototype cooling reservoir is very similar to those obtained by the numerical experiments.

In the present numerical experiments, the flow field in the cooling chamber is sensitive to the value of F_0. The thickness of the heated liquid layer very clearly increases as F_0 is increased. These phenomena were also observed in the experiments conducted by Tamai, Wiegel, and Tornberg[27] and Hayashi and Shuto.[12] Their experiments were performed for a warm-water jet discharged horizontally at the surface of a body of deep water. The dimensionless parameters considered by Tamai et al. of F_0 ranged from 2.4 to 11.3 and of R_0 ranged from 6.6×10^3 to 2.1×10^4. Those described by Hayashi and Shuto are of $F_0 = 1.4$ to 16.1 and $R_0 = 5.6 \times 10^3$ to 3.1×10^4. Tamai et al. and Hayashi et al. observed that for small values of $F_0 \leq 2.6$, a narrow stream of warm water formed along the surface, with very little mixing or spreading. The smaller the F_0, the thinner the surface layer of heated water. These phenomena were also observed in the present numerical experiments, as shown in Figures 2 and 3.

In another study, Stefan[3,24] and Stefan and Schiebe[25] presented laboratory results for heated jets entering a basin. The inlet-jet dimensions in the study were much smaller than the basin depths. Vertical isotherm plots were presented along the jet centerline for F_0 of 0.62 and 0.72. These plots indicate large temperature gradients and significant vertical convection near the inlet wall; a stratified warm layer forms near the surface away from the inlet region. This behavior is similar to that shown for the present numerical experiments for small F_0 (Figures 2a, 2b, 3a, and 3b). Their temperature gradients were larger than the numerical results obtained here. This is believed to have been due to the 2-D constraint imposed on the present numerical model, which does not take into account the lateral spreading of the buoyant fluid, and thus results in too much diffusion in the vertical direction. However, in general, their vertical isotherms are very similar to those obtained by the present numerical experiments. They also presented some velocity plots that exhibited a strong current in a narrow layer near the surface with much smaller velocities beneath this layer; some of the velocities near the bottom are in the opposite

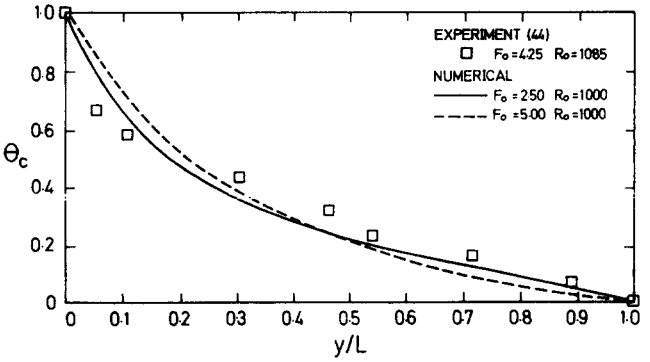

Figure 7 Comparison of observed temperature decay profiles with numerical experiments

direction to those of the surface currents. The present numerical experiments also exhibit similar behavior.

A comparison with the numerical solutions obtained by other investigators is difficult, since similar numerical solutions are not available. The velocity vector solutions obtained by Roberts and Streets[20] for heated water discharged into a simulated "sloping-dam" provided some features for comparison. Their results show the development of the flow over time. The R_0 of the flow is about 100 and the F_0 is estimated to be around 0.4. Hence, the heated water is highly buoyant. As it enters the dam, it spreads out, rises to the surface almost immediately, and moves across the dam in a surface current. The density current is then forced down to the outflow and a circulation pattern begins to form in response to the entrainment of fluid. The driving by the viscous forces originating from the surface layer flow and the downward movement of the fluid near the outlet region further enhances the circulation. These phenomena are also observed in the present numerical experiments for small F_0, as shown in Figures 2a and 3a for a rectangular cooling chamber.

Conclusions

Numerical experiments showed that the flow fields and temperature profiles in a flow-through rectangular cooling chamber are strong functions of both F_0 and R_0. Variation of F_0 has a significant effect on the trajectories of the buoyant inflow. Numerical experiments show that the thickness of the heated liquid layer increases as the F_0 is increased. The behavior for the increase in R_0 (with fixed F_0) is qualitatively similar to that for a decrease of F_0 with R_0 held constant. For the opened cooling chamber considered here, with the heated fluid discharged into the chamber near the surface, the exposure of the upper surface of the incoming heated fluid to the atmosphere results in a larger temperature excess near the surface, and thus allows greater temperature reduction by surface heat loss.

Acknowledgments

The author gratefully acknowledges the financial support of a National University of Singapore Research Grant (No. RP33/84) and the assistance of W. M. Ong and S. J. Yap during the course of this project.

References

1 Barry, R. E. and Hoffman, D. P. Computer model for thermal pollution. *J. Power Div., ASCE*, 1972, **92**(P01), 117–132

2 Boericke, R. R. and Hall, D. W. Hydraulics and thermal dispersion in an irregular estuary. *J. Hydr. Div., ASCE*, 1974, **100**, 85–102

3 Stefan, H. Modelling spread of heat water over lake. *J. Power Div., ASCE*, 1970, **96**(P03), 469–482

4 Coulter, C. G., Guthrie, A., Kirkwood, J. B., Lamb, A. N. and Watson, K. S. Thermal discharge from power stations. Conference on Thermal Discharge: Engineering and Ecology, 1972, Institute of Engineers, Sydney, Australia, 37–45

5 Edinger, J. E. and Geyer, J. C. Heat exchange in the environment. Edison Electric Institute Publication No. 65-902, 1972

6 Edinger, J. E., Euttweiler, D. W., and Geyer, J. C. The response of water temperature to meteorological conditions. *Water Resources Res.*, 1968, **4**(5), 1136–1142

7 Edinger, J. E. and Geyer, J. C. Analyzing steam electric power plant discharges. *J. Sanitary Eng. Div., ASCE*, 1968, **94**(SA4), 611–622

8 Farrow, D. E. Convective circulation in reservoir sidearms of small aspect ratio. Proceedings of Tenth Austrialasian Fluid Mechanics Conference, University of Melbourne, 11–15 December 1989, 15.41–14.43

9 Harbeck, G. E. The use of reservoirs and lakes for the dissipation of heat. *U.S. Geol. Survey Circ.* 1953, **282**, 1–9

10 Harbeck, G. E., Koberg, G. E., and Hughes, G. H. The effect of the addition of heat from a power plant on the thermal structure and evaporation of Lake Colorado City, Texas. Prof. paper 272-B, U.S. Geological Survey

11 Harleman, D. R. F. and Stolzenbach, K. D. Fluid mechanics of heat disposal from power generation. *Annu. Rev. Fluid Mech.*, 1972, **4**, 7–32

12 Hayashi, T. and Shuto, N. Diffusion of warm water jets discharged horizontally at the water surface. *Proc. 12th Congress of Int. Assoc. for Hydraulic Research, Colorado State University, Fort Collins, CO*, 1967, **4**, 47–59

13 Hayashi, T., Shuto, N., and Kawakami, K. Basic study on the diffusion of warm water jets discharged from power plants into bays. *Coastal Eng. Jpn.*, 1967, **10**, 129–142

14 Hindley, P. D., Miner, R. M., and Cayot, R. Thermal discharge: a model-prototype comparison. *J. Power Div., ASCE*, 1971, **97**(P04), 783–798

15 Jen, Y., Wiegel, R. L., and Mobarek, I. Surface discharge of horizontal warm-water jet. *J. Power Div., ASCE*, 1966, **92**(P02), 1–30

16 Jobson, H. E. The dissipation of excess heat from water systems. *J. Power Div., ASCE*, 1973, **99**(P04), 89–103

17 Koh, R. C. Y. Two-dimensional surface warm jets. *J. Hydr. Div., ASCE*, 1971, **97**, 819–836

18 Parker, F. L. and Krenkel, P. A. Physical and engineering aspects of thermal pollution. Thermal pollution: Status of the art. Report No. 3, Department of Environmental and Water Resources, Vanderbilt University

19 Paul, J. F. and Lick, W. J. A numerical model for a three-dimensional, variable-density jet. Report No. FTAS/TR-7B-92, Division of Fluid, Thermal and Aerospace Sciences, School of Engineering, Case Institute of Technology

20 Roberts, B. R. and Street, R. L. Two-dimensional, hydrostatic simulation of thermally-influenced hydrodynamics flows. Technical Report No. 194, Civil Engineering Department, Stanford University, Stanford, CA

21 Sengupta, S. and Lick, W. J. A numerical model for wind driven circulation and temperature fields in lakes and ponds. Report No. FTAS/TR-74-99, Division of Fluid, Thermal and Aerospace Sciences, School of Engineering, Case Institute of Technology

22 Snider, D. M. and Viskanta, R. Thermal stratification by radiation in surface layers of stagnant water. ASME paper No. 74-HT-44, Thermophysics and Heat Transfer Conference, Boston, MA, 1974

23 Spraggs, L. D. and Street, R. L. Three-dimensional simulation of thermally-influenced hydrodynamic flows. Technical Report No. 190, Civil Engineering Department, Stanford University, Stanford, CA, 1975

24 Stefan, H. Three-dimensional jet-type surface plumes in theory and in the laboratory. Project Report No. 126, St. Anthony Falls Hydraulic Laboratory, University of Minnesota, Minneapolis, MN, 1971

25 Stefan, H. and Schiebe, F. R. Experimental study of warm water flow into impounds, Part III. Temperature and velocity fields near a surface outlet in three-dimensional flow. Project Report No. 103, St. Anthony Falls Hydraulic Laboratory, University of Minnesota, Minneapolis, MN, 1968

26 Summers, W. R., Ellyett, C. D. and Kennewell, J. Infra-red scanning techniques applied to quantitative analysis of thermal plumes. Conference on Thermal Discharge: Engineering and Ecology, Institute of Engineers, Sydney, Australia, 1972, 46–51

27 Tamai, N., Wiegel, R. L., and Tornberg, G. F. Horizontal surface discharge of warm water jets. *J. Power Div., ASCE*, 1969, **95**(P02), 253–276

28 Bejan, A. and Tien, C. L. Laminar natural convection heat transfer in a horizontal cavity with different end temperatures. *ASME J. Heat Transfer*, 1978, **100**, 641–647

29 Catton, I. Natural convection in enclosures. *Proceedings of 6th International Heat Transfer Conference*, Toronto, Canada, Vol. 6. Hemisphere Press, Washington, D.C., 1978, 13–31

30 Chen, K. S., Ho, J. R., and Humphrey, J. A. C. Steady, two-dimensional, natural convection in rectangular enclosures with differently heated walls. *ASME J. Heat Transfer*, 1987, **109**, 400–406

31 Chung, K. C. and Trefethen, L. M. Natural convection in vertical stack of inclined parallelogrammic cavities. *Int. J. Heat Mass Transfer*, 1985, **25**(2), 277–284

32 Davalath, J. and Bayazitoglu, Y. Forced convection cooling across rectangular blocks. *ASME J. Heat Transfer*, 1987, **109**, 321–328

33 Guj, G. and Stella, F. Numerical solutions of high-Re recirculating flows in vorticity–velocity forms. *Int. J. Numerical Methods Fluids*, 1988, **8**(4), 405–416

34 Iyican, L., Bayazitoglu, Y., and Witte, L. C. An analytical study of natural convective heat transfer within a trapezoidal enclosure, *ASME J. Heat Transfer*, 1980, **102**, 640–647

35 Iyican, L., Witte, L. C., and Bayazitoglu, Y. An experimental study of natural convection in trapezoidal enclosures. *ASME J. Heat Transfer*, 1980, **102**, 648–653

36 Lam, S. W., Gani, R., and Symons, J. G. Natural convection in trapezoidal cavities, 3rd Australian Conference on Heat and Mass Transfer, University of Melbourne, May 1985, 87–94

37 Lee, T. S. Computational and experimental studies of convective fluid motion and heat transfer in inclined non-rectangular enclosures. *Int. J. Heat Fluid Flow*, 1984, **5**(1), 29–36

38 Nielsen, P. V. Flow in air conditioned rooms. Ph.D. Thesis, Danfoss A/S, Nordborg, Denmark

39 Oberkampf, W. L. and Crow, L. I. Numerical study of the velocity and temperature fields in a flow through reservoir. *ASME J. Heat Transfer*, 1976, 353–359

40 Ozoe, H., Mouri, A., Ohmuro, M., Churchill, S. W., and Lior, N. Numerical calculations of laminar and turbulent natural convection in water in rectangular channels heated and cooled isothermally on the opposing walls. *Int. J. Heat Mass Transfer*, 1985, **28**(1), 125–138

41 Ozoe, H., Mouri, A., Hiramitsu, M., Churchill, S. W., and Lior, N. Numerical calculation of three-dimensional turbulent natural convection in a cubical enclosure using a two-equation model for turbulence. *ASME J. Heat Transfer*, 1986, **108**, 806–813

42 Patankar, S. V. Recent developments in computational heat transfer. *ASME J. Heat Transfer*, 1988, **110**(4B), 1037–1045

43 Patterson, J. C. Unsteady natural convection in a cavity with internal heating and cooling. *J. Fluid Mech.*, 1984, **140**, 135–140

44 Pleasance, G. E. Heat transfer in stratified flow. Masters of Engineering Thesis, School of Civil Engineering, University of New South Wales, Sydney, Australia

45 Poulikakos, D. and Bejan, A. The fluid mechanics of an attic space. *J. Fluid Mech.*, 1983, **131**, 251–269

46 Mallinson, G. D. and de Vahl Davis, G. The method of false transient for the solution of coupled elliptic equations. *J. Comp. Phys.* 1973, **12**, 435–461

47 Behnia, M., Wolfstein, M., and de Vahl Davis, G. A stable fast marching scheme for computational fluid mechanics. *Int J. Numerical Methods Fluids*, 1990, **10**(6), 607–621

48 Peaceman, D. W. and Rachford, H. H. Jr. The numerical solution of parabolic and elliptic differential equations. *J. SIAM*, 1955, **3**, 23–41

49 Courant, R., Friedrichs, K. and Lewy, H. On partial difference equations of mathematical physics. *IBM J. Res.* 1967, 215–234